1 Motivation and Objectives

The research objective of this proposal is to predict the intracavity conditions in sonoluminescence (SL) with modelling and simulation by an integrated full hydrodynamic framework. Sonoluminescence occurs when a bubble in a liquid is acoustically driven into nonlinear radial oscillation. This non-linear radial oscillation can focus the diffuse energy of the sound field by many orders of magnitude and leads to broadband light emission (sonoluminescence) and broken molecular bonds (sonochemistry). Spectroscopic work on single-bubble sonoluminescence (SBSL) in sulphuric acid (H_2SO_4) quantified heavy-particle temperatures and pressures in excess of 15,000 K and 4,000 atm (0.4 GPa), respectively [1]. Flannigan and Suslick [1] also commented that there is experimental evidence [2] of the formation of an optically opaque core as bubble implosion proceeds. The interior core of the collapsing bubble, which is not visible by emission spectroscopy, must have conditions that exceed, perhaps markedly, temperature and electron densities measured for the outer emitting surface. *Thus, the objectives of the current proposal is to make a transformative leap in the prediction of intracavity conditions including the temperature and pressure at the maximum compression by full hydrodynamics numerical simulations, which are not limited by core opacity in experiments.*

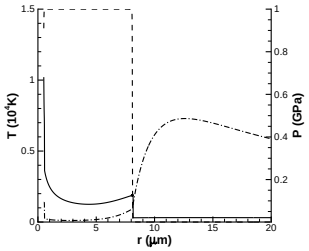

(a)

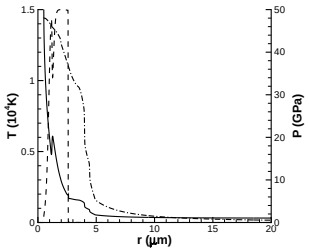

(b)

Figure 1: Plot of temperature (solid), pressure (dash-dot), and mass fraction of O_2 (dashed; between 0 and 0.23) as a function of r for numerical simulation of SL [3] at (a) 2.5 ns before the bubble rebounds when reaction just starts and (b) the moment the bubble rebounds.

The problem to be studied is multiphysics. The nonlinear radial oscillation in sonoluminescence involves highly compressible two-phase hydrodynamics and strong GPa shock waves, phase change at the liquid-vapor interface, air/vapor chemistry inside the bubble, non-ideal equation of state at high GPa pressure, thermal diffusion and species diffusion/dissolution, noble gas content, plasma and radiation and so on. The modeling of most of these physics will be challenging in themselves so we will incorporate them strategically and explore models at different levels of fidelities at different stages of the proposed research balanced between the accuracy of the models and tractability of computational complexity and intensity.

The problem to be studied is also intrinsically multiscale. The length scale of the acoustic excitation is on the order of centimeter while the length scale of the bubble micron. In addition, the length and time scale of the expansion phase of sonoluminescence are on the order of tens of micron and micro-second, respectively, whereas those of the final maximum compression phase can be micron and nano- to pico-second. The strategy to overcome this difficulty in full hydrodynamic simulations has been a two step calculation whereby the bubble expansion was simulated in Step 1 either with Rayleigh-Plesset model or a full hydrodynamic framework with timestep and grid size appropriate for acoustic excitation. The results obtained from Step 1 were then used as the initial conditions for Step 2 at tens of ns before the final collapse. We showed in [3] that dissociation of air and water vapor does not start until a few ns before the final collapse (Fig. 1). Therefore, it seems to be justifiable to neglect the evolution of bubble expansion but start a full-hydrodynamic simulation tens of ns before the collapse with rationally assumed initial conditions and chemical compositions from Step 1. We will, however, study vaporization, diffu-

sion, dissolution, etc. during the acoustic excitation phase as well to obtain more accurate initial condition for Step 2 simulation discussed above.

Therefore, we accomplish the objectives of the proposed research through the following components:

1. **Modeling and implementation of physics involved.** Various physics discussed above will be modeled at again different levels of fidelities at different stages of the proposed research. Phase transition modelling with mass and heat transfer at the liquid-vapor interface will be incorporated first into our existing multi-phase full hydrodynamic reactive flow solver. This will enable the simulation of vaporization at the expansion phase of sonoluminescence and provide a more accurate condition inside the bubble before its collapse. For the collapse phase, air and water vapor chemistry, plasma physics, radiation etc. will need to be included. Recently, we were the first to include dissociation of air and water vapor in a full hydrodynamic simulation of SBSL [3]. This reactive flow solver will be extended to account for more and adequate number of reactions for air and water vapor chemistry. Plasma physics will be incorporated either through approximate thermodynamics and transport property models at adequate fidelity or moderately detailed plasma-hydro coupling and plasma chemistry if needed for comparison with experimental observation.

2. **Comparison to experimental data of the light emission from sonoluminescence.**

   Once various physics discussed in Stage 1 above are incorporated and verified, simulations of SBSL will be performed, and spectroscopic features such as pulse width and spectra will be extracted from the simulation data as post-processing for comparison with the experimental light emission from sonoluminescence. There are also other observables that can be used for validation of our model such as the number of radicals such as OH dissolving into the surrounding liquid from the interior of the bubble.

3. **Predictive modeling for S/MBSL and outlook for cavitation erosion.**

   A direct predictive outcome of the validated model of SBSL in Stage 2 are the intracavity conditions including the temperature and pressure at the maximum compression. The next predictive modeling will be intracavity conditions and bubble interaction in multi-bubble sonoluminesence (MBSL). The non-spherical nature defies concise analytical treatment of MBSL so significantly less numerical and theoretical work have been done for MBSL. Finally, the acoustic excitation simulation with SBSL provides valuable knowledge base for cavitation erosion.

2 Backgrounds

Sonoluminescence was first discovered in 1933 by Marinesco and Trillat [4] who noted that photographic plates immersed in water fogged when irradiated by ultrasound. The next year Frenzel and Schultes [5] directly observed sonoluminescence in water. Sonoluminescence involves the conversion of acoustical to optical energy. Through the application of an acoustic field, a bubble can be created by the expansion wave of the sound field. The bubble will grow and contract with the cycling of the acoustic field. With acoustic fields of sufficient amplitude, the expansion and compression cycle becomes highly nonlinear. The runaway inertial collapse and compression of bubble contents leads to a flash of light that lasts tens of picoseconds to a few nanoseconds. The conditions inside the bubble can be extreme. Temperatures inside the bubble can

reach 15,000 K, and pressures can reach GPa [1]. Flannigan and Suslick [1] also commented that there is experimental evidence of the formation of an optically opaque core as bubble implosion proceeds. Thus, the interior core of the collapsing bubble must have conditions that exceed, perhaps markedly, temperature and electron densities measured for the outer emitting surface. Therefore, there are still questions as to what the true intracavity conditions in SL are.

The emission of high-pressure pulses by a collapsing bubble, which originates from a strong compression of the bubble contents, has been well known since the famous theoretical work of Rayleigh [6] on an imploding spherical cavity. Developed by Rayleigh [6] and refined by Plesset [7], the Rayleigh-Plesset (R-P) model is one of the most predominant models used to describe sonoluminescence. R-P model, shown in equation (1), is an ordinary differential equation of the bubble radius $R(t)$.

$$R\ddot{R} + \frac{3}{2}\dot{R}^2 = \frac{1}{\rho}[P_B(t) - P_\infty(t) - \frac{2\sigma}{R} - \frac{4\mu\dot{R}}{R}] \tag{1}$$

where R is the bubble radius (dots represent first and second derivatives), ρ is the bulk liquid density, P_B is the bubble pressure, P_∞ is the far-field pressure, σ is the surface tension, μ is the shear viscosity. Among the assumptions used to derive R-P are (1) a constant spherical symmetry of the bubble, (2) the density of the liquid is larger than the gas density within the bubble, (3) isothermal liquid [8], (4) homogeneous pressure inside the bubble [8], and (5) uniform contents in the bubble [9]. R-P is able to produce accurate results over most of range of bubble motion [10,11], but is severely limited with increasing bubble compression and eventual bubble collapse [8]; the assumptions are no longer valid at maximum compression and collapse [8,11,12]. Improvements to the R-P model by incorporating sound radiation, van der Waals hard core law, and retarded time has resulted in advanced models such as Gilmore and Keller-Miksis (K-M) [13]. The underlying assumptions of R-P are also presented in these more advanced models; the accuracy of the models for bubble motion away from maximum compression and collapse is better. However, the theoretical work becomes insufficient since the assumptions depart from the actual bubble conditions at times of maximum compression. One such assumption is that the density of the liquid is much larger than the gas density within the bubble, which is not true during the bubble collapse when the bubble approaches the minimum radius for a strongly driven bubble.

The relative ease in incorporating various physics involved and affordable computational cost of R-P based model makes it attractive. There are abundant numerical studies that solve the R-P model with various physical and chemical processes included [14–20]. Yasui [14] and Yasui *et al.* [15] extended the R-P based model to include fairly detailed vapor and air chemistry, dissolution, vaporization/condensation etc. Schanz *et al.* [17] studied the sonochemistry using a combination of R-P and molecular dynamics (MD). Prosperetti reviewed the fundamental physics of vapor bubbles in liquids [20]. Full hydrodynamic numerical simulations of SBSL with the compressible equations do not have the limitations of R-P model yet the amount of these simulations is severely limited. To the best of our knowledge, Wu and Roberts [21] and Moss *et al.* [22, 23] are amongst the first attempts at a full hydrodynamic simulation of SBSL. Therefore, we will make an effort in this proposed research to enhance the simulation database for SBSL. In addition, the sophistication in terms of the amount and details of various physics involved in SL in full hydrodynamic numerical framework lags significantly behind the R-P based models. Therefore, there is a need for advancement in the capabilities of full hydrodynamic numerical framework for simulations of SBSL. The advancement will in particular enable the examination of the effect of spatial variation. The advancement is also needed for simulation of MBSL and

other applications such as cavitation erosion that can not be simulated by R-P based model.

As such, various physics involved in SL will be incorporated in the proposed research. The main numerical framework/code we developed [24, 25] is based on the HLLC finite volume and the diffuse interface-capturing scheme by Shukla *et al.* [26]. The multiphase compressible flow solver can handle different microstructures, strong shocks, multi-material/phase interfaces, material deformation, general equations of state (EOS), and chemistry. As a first step towards the ultimate goal of simulating SL, we recently made an effort in [3] to incorporate air and water vapor chemistry and equation of state for air at high pressures. It was shown that for sonoluminescence they indeed have significant effects on the peak temperature and pressure attained during the evolution as shown in Fig. 2. Therefore, accurate prediction of intracavity conditions in SL indeed relies on an integrated full hydrodynamic numerical framework with important physics accounted for.

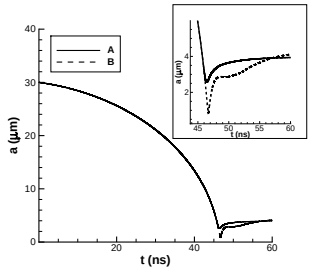

(a)

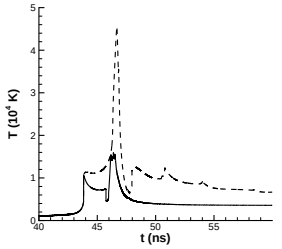

(b)

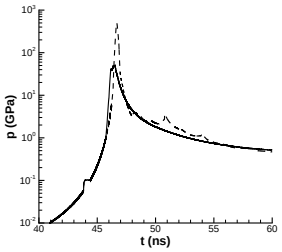

(c)

Figure 2: Evolution of (a) radius with an inset showing the evolution near the collapse, (b) maximum temperature, and (c) maximum pressure for bubble collapse in spherical symmetry and for cases with air chemistry and equation of state for air at high pressures (solid) and without (dash) [3].

Thus, as discussed in the Objectives section, various physics discussed above will be modeled at again different levels of fidelities at different stages of the proposed research. Also, as discussed in the Objectives section, due to the multi-scale nature and the high computational cost for full hydrodynamic simulations, the calculation will be divided into two steps, the acoustic excitation/expansion phase and the final collapse phase. For the acoustic excitation/expansion phase, phase transition modelling for evaporation/condensation with mass and heat transfer at the liquid-vapor interface based on [27–29] will be incorporated first into our existing multi-phase full hydrodynamic reactive flow solver. As will be explained in more detail later, at each time step, the hyperbolic system in the absence of heat and mass transfer is solved. This provides the non-equilibrium hydrodynamic field. Stiff thermal and chemical relaxations (for vaporization) are then solved at the interfaces only. Phase transition modelling has never been done for SL in full hydrodynamic framework. This capability will enable the simulation of vaporization at the expansion phase of sonoluminescence and provide more accurate conditions including the vapor contents inside the bubble before its collapse. This is important for the simulation of water vapor chemistry and accurate simulated number of radicals such as OH dissolving into the surrounding liquid from the interior of the bubble in the collapse phase for comparison with the experiments.

For the collapse phase, the existing reactive flow solver in [3] will be extended to account for adequate number of reactions for air and vapor chemistry based on those in the R-P model in [15]. However, since each reaction will add one more (or two if both the forward and reverse reactions are considered) governing equations to the full hydrodynamic system, a reduced model like in [30] with eight species and nine reactions may be pursued first.

The direct observation of noble-gas ion emission lines (for example, Xe^+ , Kr^+ and Ar^+)

provided definitive evidence for generation of plasma during SL [31]. Therefore, it is necessary to include plasma physics and noble gas content in numerical simulations of SL. Plasma physics will be incorporated either through approximate thermodynamics and transport property models like in [23,32] at adequate fidelity or moderately detailed plasma-hydro coupling and plasma chemistry like in [33,34] as needed for comparison with experimental observation. Alternatively, energy change due to plasma can also be modeled as a source term similar to that in the R-P model in [35].

In summary, similar to the framework for complex plasma-combustion system in [33], because of the many potentially important interactions of physics in SL, the model is designed specifically *not* to provide the ultimate, highest-fidelity possible representations of any of the mechanisms. Instead, as noted in [33], it is designed with three general criteria in mind: (1) that it be physics based, expressible as approximations of more fundamental or more detailed physics; (2) that it represents all the principal anticipated phenomenology in the corresponding system; and (3) that its numerical evaluation does not fundamentally increase the computational intensity beyond that of the corresponding inert flow. *This integrated framework will however represent a transformative leap and the state of the art in full hydrodynamics predictive modeling of SL with the most complete set of physics that have not been examined before.*

Once the various physics are incorporated and the integrated framework verified, simulations of SBSL will be performed, and spectroscopic features such as pulse width and spectra will be extracted from the simulation data as post-processing like in [36–39] for comparison with the experimental light emission from sonoluminescence such as those in [1, 31, 40, 41]. A direct predictive outcome of the validated model of SBSL will be the intracavity conditions including the temperature and pressure at the maximum compression, that were not observable in experiments due to the formation of an optically opaque core as bubble implosion proceeds [1].

The next predictive modeling will be intracavity conditions and bubble interaction in multi-bubble sonoluminesence (MBSL). The non-spherical nature defies concise analytical treatment of MBSL. Also, a broader impact of the proposed research would be cavitation erosion. Significantly more full hydrodynamic simulations were performed for interaction of a bubble and a shockwave for the obvious reason again that the complexity in these interaction defies concise analytical treatment; see [42–48] and references therein. This leaves numerical methods as the foremost means of studying shock-bubble interaction and cavitation erosion. However, in all of these simulations, acoustic excitation phase in cavitation erosion was by-passed due to the larger length and time scale in that phase and the lack of phase transition modeling. Thus, the acoustic excitation simulation for SBSL with the proposed framework provides valuable knowledge base for cavitation erosion. Simulation and research on cavitation process can be done by starting the simulation with acoustic excitation and relaxing the assumption that shock has been generated. Thus, the mechanisms of shock generation and damaging in cavitation erosion may be identified.

3 Research Methods

3.1 Base Model for Multiphase Compressible Flow

An in-house code has been developed, verified and validated over a number of years for multiphase compressible flows with a diffuse interface model [3, 24, 25]. The numerical solver can handle different microstructures, strong shocks, multi-material/phase interfaces, material deformation, general equations of state (EOS), and chemistry. The governing equations for a three-dimensional reactive

medium are solved,

$$\frac{\partial(\rho_1\phi)}{\partial t} + \nabla\cdot(\rho_1\phi\boldsymbol{u}) = 0, \qquad \frac{\partial(\rho_2(1-\phi))}{\partial t} + \nabla\cdot(\rho_2(1-\phi)\boldsymbol{u}) = 0, \qquad \frac{\partial(\rho\boldsymbol{u})}{\partial t} + \nabla p + \nabla\cdot(\rho\boldsymbol{u}\boldsymbol{u}) = 0,$$

$$\frac{\partial E}{\partial t} + \nabla\cdot((E+p)\boldsymbol{u}) = \Sigma Q_i\Omega_i, \qquad \frac{\partial(\rho Y_i)}{\partial t} + \nabla\cdot(\rho\boldsymbol{u}Y_i) = -\Omega_i, \tag{2}$$

Here, ϕ is the volume fraction of material 1, and $(1-\phi)$ the volume fraction of material 2; ρ_1 and ρ_2 are the densities of material 1 and 2, respectively. The total density is obtained as $\rho = \rho_1\phi + \rho_2(1-\phi)$. In addition, $\boldsymbol{u}$ is the velocity, p the pressure, $E = \rho\left(e + \frac{1}{2}\boldsymbol{u}\cdot\boldsymbol{u}\right)$, the total energy per unit volume, Y_i the mass fraction of the i^{th} reactant, and Q_i a heat release parameter. See Sec. 5.2 for chemistry.

Finally, the system is closed by adding appropriate equation of state,

$$p = p(\rho, e). \tag{3}$$

The EOS can be an ideal gas EOS, a stiffened EOS or a Mie-Gruneisen EOS.

The Euler equations above are solved in conservative form using the common reconstruct-and-evolve strategy within a finite-volume framework. In addition, a TVD reconstruction with the Minmod limiter [49] is employed. The HLLC approximate Riemann solver [50] is chosen for its good resolution of shocks and its positivity of density and internal energy. Time integration is performed using a strong-stability-preserving third-order Runge-Kutta method [51]. See Shukla *et al.* [26] for more details (see [24] for the extension to reacting flows).

3.2 Diffuse Interface Model

The particular problems we are addressing have chemical reactions, shock waves, and material interfaces, and therefore an appropriate numerical method must be capable of handling all of them. A numerical method was recently developed by Shukla *et al.* for handling such problems [26], albeit in the absence of chemistry.

A key ingredient in multi-material modeling in [26] is the use of a material marker ϕ, advected according to

$$\frac{\partial\phi_k}{\partial t} + \mathbf{u}\cdot\nabla\phi_k = 0. \tag{4}$$

Here, ϕ_k is the volume fraction of material k, such that $\sum\phi_k = 1$. In the physical system ϕ_k jumps from 0 to 1 across a material interface, but in the numerical scheme it changes smoothly over a small number of mesh points, a set S. Over a time step Δt, ϕ_k is advanced using equation (4). Upwind fluxes for the advection equation for the interface function ϕ_k are calculated as a part of the two-fluid Riemann problem using the contact velocity from the HLLC solver.

Over a time step Δt, ϕ is advected using (4), but before moving to the next time step a correction is calculated on $\mathcal{S}$ by means of the equation

$$\frac{\partial\phi}{\partial\hat{\tau}} = \hat{n}\cdot\nabla\left(\epsilon_h|\nabla\phi| - \phi(1-\phi)\right), \tag{5}$$

where $\hat{\tau}$ is a pseudo-time and $\hat{n}$ is the interface normal. This equation is integrated to steady state in $\hat{\tau}$. The nonlinear term leads to convective steepening of the interface region, whereas the diffusion term smears it out; these effects balance, as in Burger's equation.

The density ρ is treated in a similar fashion using

$$\frac{\partial\rho}{\partial\hat{\tau}} = H(\phi)\hat{n}\cdot\left(\nabla(\epsilon_h\hat{n}\cdot\nabla\rho) - (1-2\phi)\nabla\rho\right), \tag{6}$$

where, $H(\phi) = \tanh\left[\left(\frac{\phi(1-\phi)}{10^{-2}}\right)^2\right]$. The Heaviside function $H(\phi)$ ensures that the density correction step is limited to the interface region. This scheme was fully demonstrated in [26], and for reacting flows in [24]; see also [52, 53]. A mass and volume conserving interface reinitialization scheme for a diffuse interface has also been proposed recently [54], where a Lagrange multiplier λ_ρ was introduced to the density correction Eqn. (6) and calibrated to conserve the bubble mass, namely

$$\frac{\partial(\rho_1\phi_1)}{\partial\hat{\tau}} = H(\phi_1)\mathbf{n}\cdot(\nabla(\epsilon_h\mathbf{n}\cdot\nabla(\rho_1\phi_1)) - (1-2\phi_1)\nabla(\rho_1\phi_1)) + H(\phi_1)\lambda_\rho, \tag{7}$$

where ρ_1 is the bubble density. Thus, ρ_1 is adjusted within the set S to precisely preserve the bubble mass, independent of grid resolution. We do note that, for deformation dominant problem like in bubble collapse, the solution with mass conservation correction (7) is essentially identical to that by the original scheme without mass conservation correction, the only noticeable difference being in density in the air near the interface. Thus, the bubble mass conservation in bubble collapse simulation seems to be only an issue of post-processing due to the difficulty in defining the boundary of the bubble and the large density contrast across the interface during integration over the volume of the bubble in diffuse interface method.

3.3 Equation of State

A stiffened-gas EOS is used for closure and is given by,

$$\rho_k e_k = \Gamma_k p_k + \Pi_k, \tag{8}$$

with $\Pi_k = \frac{\gamma_k p_k^\infty}{\gamma_k - 1}$, $\Gamma_k = \frac{1}{\gamma_k - 1}$. Here, γ is a parameter and p^∞ is a constant. Both can be calibrated for a certain material. Note that in the limit $p^\infty \to 0$ the stiffened EOS reduces to the ideal EOS and γ becomes the ratio of specific heats.

With the volume fraction ϕ known, the EOS parameters of the mixture can then be obtained. The isobaric closure of Allaire *et al.* [55] was chosen in [26] for stiffened EOS parameters.

The EOS parameters for the materials in the current work are listed in Table 1. Note that we assume in this work that the EOS for the air inside the bubble at pressures on the order of GPa and larger is stiffened. The calibration of the parameters is based on shock Hugoniot data of liquid N_2 in [56]. The use of shock data seems plausible in the current problem in which shocks with pressures on the order of GPa are present.

Parameter/Material	Water	Air ($p_{max} \leq 1$ GPa)	Air ($p_{max} > 1$ GPa)
ρ_0 (kg/m^3)	1000	1.	1000.
γ	4.4	1.4	2.6
P^∞ (atm)	6000.	0	1.07×10^4

Table 1: Parameters of the Stiffened-Gas EOS.

3.4 Packing Algorithm

As discussed in the Objectives section, predictive modeling will be performed for intracavity conditions and bubble interaction in multi-bubble sonoluminesence (MBSL) as well as cavitation erosion.

Thus, mesoscale simulations of shock passing through a random bubble cloud is relevant to examine the pressure increase associated with wave interaction. A random packing algorithm based on the Lubachevsky-Stillinger (LS) algorithm [57] can be used to generate the random bubble cloud; see [58, 59] for details. The LS dynamic packing algorithm randomly places N zero radii spheres in the domain. Using the largest diameter for nondimensionalization, the domain is scaled to a unit cube. The spheres are then given a random velocity sample from a fixed temperatured Maxwell-Boltzmann distribution, grow at a preselected rate, and undergo classic (super-) elastic collision dynamics. The algorithm stops when a specified packing fraction or jamming criterion is reached. To increase the efficiency and application of the algorithm, an event-driven molecular dynamic approach and a hierarchical cell structure [58] and the level set methods [59], respectively, were implemented. Figure 3 shows an example of polydispersed random bubble cloud generated with the packing algorithm.

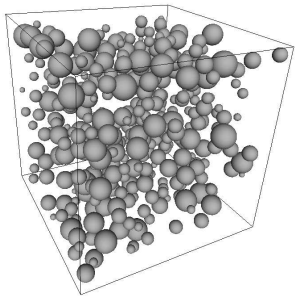

Figure 3: An example of polydispersed random bubble cloud generated with the packing code.

4 Previous Results - Capability Demonstration

We now demonstrate the key capabilities of the numerical framework to be used in the proposed work. We show a series of example validation results from [3,25] by our numerical tool.

The single bubble collapse test problem in [52] is simulated. In this problem, the collapse of a spherical air bubble in water under an initial pressure ratio $p_\infty/p_0 = 25$, with p_∞ of 10^5 Pa and the bubble at its maximum radius $R_0 = 1$ mm at $t = 0$, is considered. The initial pressure in the water is $p(r) = p_\infty + \frac{R_0}{r}(p_0 - p_\infty)$. A domain of [0:200] mm with 16000 grid points is used in the current simulation. The CFL number is 0.5. The solution is compared to that by [60] in Figure 4. Excellent agreement is obtained.

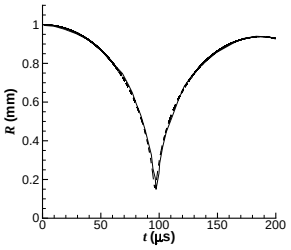

Figure 4: Plot of bubble radius R as a function of time: semi-analytical solution of [60] (solid) and current simulation (dashed).

Fig. 5 in [25] next demonstrates the capability of our code in simulating shock particle interaction and the comparison with the experimental results of [61].

4.1 Sonoluminescence

Bubble collapse in spherical symmetry corresponding to an initial bubble radius of $R_0 = 30$ μm in water is simulated. The initial conditions are chosen to be representative of those for Step 2 in [22], and v_r is 0 inside and -100 m/s outside the bubble initially. Note that the inner boundary of the domain is set to $r_0 = 0.05$ μm to remove the singularity at $r = 0$; our solutions are insensitive to this choice provided it is sufficiently small (results not shown). The initial mass fraction of O_2 and N_2 in the bubble are 0.233 and 0.767, respectively. The stiffened-gas EOS parameters are listed in Table 1.

Figure 1 plots the temperature, pressure, and mass fraction of O_2 at various times. It can be seen that the first peak in temperature and pressure shown in Fig. 2 correspond to the moment when the

shock reaches the inner boundary of the bubble; i.e., panel (a) of Figure 1. The second peak corresponds to the moment of rebounding; i.e., panel (b) of Figure 1.

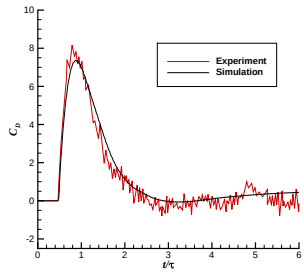

Figure 5: Plot of drag coefficient C_D as a function of nondimensional time t/τ for shock Al particle interaction in air in [25]. Here, the experimental results of [61] are shown in red.

We next examine the combined effects of the equation of state and air chemistry at high pressures inside the bubble. Two cases are simulated. Case A includes both stiffened gas EOS at high pressure and air chemistry, whereas case B does not. Figure 2 plots the bubble radius, maximum temperature, and maximum pressure as a function of time and for both cases A and B. It can be seen from the figure that air chemistry and the equation of state at high pressure has a significant effect on the peak temperature and peak pressure attained during the evolution. In particular, the maximum temperature is appreciably lower when air chemistry is included. Also, the stiffened EOS inside the bubble increases the stiffness of the bubble, thereby significantly increasing the radius at the time of rebound, which in turn reduces the peak bubble pressure by an order of magnitude. We comment that the peak temperature for case A is on the order of 1 eV, which is close to that observed in sonoluminescence [62], and the peak pressure is on the order of 100 GPa.

4.2 Shock Bubble Interaction

A numerical simulation of axisymmetric bubble collapse in water was also performed in [3], and it was shown that the temperatures inside the bubble with air chemistry are appreciably lower than those without air chemistry, indicating the effect of dissociation of air molecules.

Fig. 6a) shows a preliminary mesoscale 3-D simulation of a 1 GPa shock hitting a random bubble cloud ($d = 10$ μm), and Fig. 6b) plots the comparison of the evolution of maximum pressure for shock-single-bubble (red) and shock-random-bubble-cloud simulations. The increase in maximum pressure due to wave interaction in bubble cloud and thus higher damaging potential is demonstrated. The effect of wave interaction on pressure in water was examined in detail in [3] for axisymmetric geometry. Further systematic research on e.g. the effects of bubble size distribution and "packing fraction" on increase in pressure will be conducted in the proposed work.

4.3 AMR Capabilities

We have recently enhanced our three-dimensional multiphase solver with the Adaptive-Mesh-Refinement (AMR) capabilities through Boxlib [63, 64]. AMR is crucial to the capability of simulating bubble dynamics. This is especially true when in the long run we would like to simulate the acoustic excitation where size of the flow domain needs to be orders of magnitude larger than the size of a bubble. Boxlib, developed by the Center for Computational Sciences and Engineering (CCSE) at Lawrence Berkeley National Laboratory (LBNL) is used to implement the AMR data structure and multi-level interpolation/restriction. Boxlib is chosen for its "massively parallel, block structure AMR" capabilities.

5 Proposed Research and Development

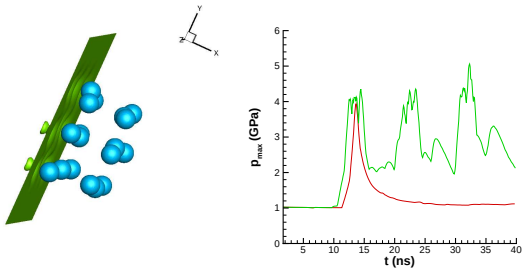

(a) (b)

Figure 6: (a) Iso-contours of density of shock-random-bubble-cloud interaction simulation. (b) The corresponding evolution of maximum pressure (green) compared with that for shock-single-bubble (red).

As discussed in the Objectives section, there is experimental evidence of the formation of an optically opaque core as bubble implosion proceeds. The interior core of the collapsing bubble, which is not visible by emission spectroscopy, must have conditions that exceed, perhaps markedly, temperature and electron densities measured for the outer emitting surface. We therefore propose to numerically investigate the mechanisms behind sonoluminescence and predict the intracavity conditions in sonoluminescence (SL) with modelling and simulation by an integrated full hydrodynamic framework.

The proposed work are outlined in the following list:

- Modeling and implementation of physics involved (1-2 years; a Ph.D. student on phase-transition modeling and a Postdoctral Fellow on various physics for the final collapse phase)
- Comparison to experimental data of the light emission from sonoluminescence (1 year overlapping with item 1)
- Predictive modeling for S/MBSL and outlook for cavitation erosion. (1 year after item 1 and years beyond)

5.1 Phase-transition Modeling for Bubble Expansion/Acoustic Excitation

Phase transition modelling important for bubble expansion and acoustic excitation with mass and heat transfer at the liquid-vapor interface will be incorporated first into our existing multi-phase full hydrodynamic reactive flow solver presented in the previous section. Phase transition has never been modeled for SL in full hydrodynamic framework so the effort will make a transformative leap. A hyperbolic two-phase flow model [27] involving five partial differential equations with two temperatures and entropies but a single pressure and a single velocity is solved. The modified equations (only) in the system in Eqn. (2) are,

$$\frac{\partial \phi_1}{\partial t} + \boldsymbol{u}\cdot\nabla\phi_1 = K\mathrm{div}(\boldsymbol{u}) + \frac{\phi_1\phi_2}{\phi_2\rho_1c_1^2+\phi_1\rho_2c_2^2}\left(\frac{\Gamma_1}{\phi_1}+\frac{\Gamma_2}{\phi_2}\right)Q_1 + \frac{\dfrac{\rho_1c_1^2}{\phi_1}+\dfrac{\rho_2c_2^2}{\phi_2}}{\dfrac{c_1^2}{\phi_1}+\dfrac{c_2^2}{\phi_1}}\rho\dot{\mathcal{Y}}_1,$$

$$\frac{\partial \phi_1\rho_1}{\partial t} + \mathrm{div}(\phi_1\rho_1\boldsymbol{u}) = \rho\dot{\mathcal{Y}}_1, \qquad \frac{\partial \phi_2\rho_2}{\partial t} + \mathrm{div}(\phi_2\rho_2\boldsymbol{u}) = -\rho\dot{\mathcal{Y}}_1, \tag{9}$$

where $K = \frac{\phi_1\phi_2(\rho_2c_2^2-\rho_1c_1^2)}{\phi_2\rho_1c_1^2+\phi_1\rho_2c_2^2}$, $\dot{\mathcal{Y}}_1 = \nu(\bar{g}_2-\bar{g}_1)$, and $Q_1 = H(T_2-T_1)$.

Note that the $K\text{div}(\boldsymbol{u})$ term in Eqn. 9 arises in the asymptotic limit [65] of stiff mechanical relaxation of a non-equilibrium two-phase, two-pressure and two-velocity hyperbolic multiphase flow model in [66]. Saurel *et al.* [27] extended the analysis to model phase transition with heat, Q_1, and mass, $\rho\dot{\mathcal{Y}}_1$, transfer at the transition front. Here, $\rho\dot{\mathcal{Y}}_1$ represents the mass flux from fluid 2 to fluid 1, e.g., from liquid water to vapor. Finally, $\bar{g}$ and T are the Gibbs free energy and temperature, respectively, and ν and H are the relaxation parameters. Six- or seven-equation models [28, 29] to maintain non-equilibrium of pressure (for six-equation) or both (for seven-equation) are also available for better agreement with the evaporation front velocity measured in the experiments in shock tubes by Simoes-Moreira & Shepherd [67].

Models for physics important for the final collapse phase are introduced next.

5.2 Improved Air and Water Chemistry Modelling

The current model of air chemistry at high temperature in [3] is based on [68]. In the current model, the following reactions are considered,

$$\mathrm{O_2} + M \xrightarrow{k_f} 2\mathrm{O} + M, \quad \mathrm{N_2} + M \xrightarrow{k_f} 2\mathrm{N} + M, \tag{10}$$

For dissociation of $\mathrm{O_2}$ for example, the reaction rate is given by $\frac{d[\mathrm{O}]}{dt} = 2k_f[\mathrm{O_2}][M]$, or $\frac{d[\mathrm{O_2}]}{dt} = -k_f[\mathrm{O_2}][M]$. The collision partner M for dissociation of $\mathrm{O_2}$ is chosen to be $\mathrm{O_2}$, and the reaction rate is then written in terms of mass fraction of $\mathrm{O_2}$, $Y_{\mathrm{O_2}}$, as

$$\frac{d(\rho Y_{\mathrm{O_2}}/\mathcal{M}_{\mathrm{O_2}})}{dt} = -k_f(\rho Y_{\mathrm{O_2}}/\mathcal{M}_{\mathrm{O_2}})^2, \tag{11}$$

where $k_f = C_f T^{\eta_f} e^{-K_f/\mathcal{R}T}$, with parameters based on [68] listed in Table 2. Thus, the source term due to reaction for $\mathrm{O_2}$ in Eqn. (2) is given by

$$\Omega = k_f(\rho Y_{\mathrm{O_2}})^2/\mathcal{M}_{\mathrm{O_2}}. \tag{12}$$

For dissociation of $\mathrm{N_2}$, the model is exactly the same as that for $\mathrm{O_2}$ but with the collision partner M chosen to be $\mathrm{N_2}$.

	$\mathrm{O_2}$	$\mathrm{N_2}$
$\mathcal{M}$ (g/mol)	32	28
C_f $\left(\frac{cm^3\ K^{-\eta_f}}{mol\ s}\right)$	3.24×10^{19}	4.7×10^{17}
η_f	-1	-0.5
K_f (cal/mol)	119000	226000
$\mathcal{R}$ (cal/mol K)	1.986	1.986
Q (MJ/kg)	-15.56	-33.79

Table 2: Kinetic parameters of $\mathrm{O_2}$ and $\mathrm{N_2}$ dissociation; see [68]. See [69] for values of Q.

For water vapor chemistry, our current model is based on [15] with the following reaction,

$$\mathrm{H_2O} + M \rightarrow \mathrm{HO} + \mathrm{O} + M, \tag{13}$$

and reaction rate coefficient defined as, $R_f = A_f T^{b_f} e^{-C_f/T}$, with parameters listed in Table 3. We have also cross-validated the kinetic parameters between [15] and [68] using $\mathrm{O_2}$ dissociation.

	H_2O	O_2
A_f $\left(\frac{m^3\ K^{-b_f}}{mol\ s}\right)$	1.96×10^{16}	1.58×10^{11}
b_f	-1.62	-0.5
C_f (K)	59700	59472

Table 3: Kinetic parameters of H_2O and O_2 dissociation in [15].

The reaction model above will be extended to account for adequate number of reactions for air and vapor chemistry based on those in the R-P model in Yasui *et al.* [15]. For a bubble initially consisting of nitrogen, oxygen, and argon, 93 chemical reactions and their backward reactions are considered in [15] involving N_2, O_2, H_2O, OH, H, O, HO_2, H_2O_2, O_3, N, HNO_2, HNO, HNO_3, NO, NO_2, and N_2O. However, in a full hydrodynamic system, each reaction will add one more (or two if both the forward and reverse reactions are considered) governing equations, a reduced model like in [30] for the shock-heated air surrounding a sounding rocket under flight conditions of 3.5 km/s may be pursued first, with eight species and nine reactions, $N_2 + M \leftrightarrow N + N + M, O_2 + M \leftrightarrow O{+}O{+}M, NO{+}M \leftrightarrow N{+}O{+}M, N_2{+}O \leftrightarrow NO{+}N, NO{+}O \leftrightarrow O_2{+}N, O_2{+}H \overset{k_1}{\leftrightarrow} O{+}OH, H_2O{+}N_2 \overset{k_2}{\leftrightarrow} H + OH + N_2, OH + N_2 \overset{k_3}{\leftrightarrow} H + O + N_2, H_2O + O \overset{k_4}{\leftrightarrow} 2OH$. The presence of argon as the third body in reactions will also be included.

5.3 Plasma Modeling

Plasma physics will be incorporated at different levels of fidelity, either through approximate thermodynamics and transport property models like in [23, 32] at adequate fidelity or moderately detailed plasma-hydro coupling and plasma chemistry like in [33,34] as needed for comparison with experimental observation. In [23], the internal energy equation is split into two with pressure and energy partitioned into ionic and electronic components,

$$\rho\frac{\mathrm{D}e_i}{\mathrm{D}t} = -(p_i + A)\nabla\cdot\boldsymbol{u} + \bar{K_{ie}}(T_e - T_i) + \nabla\cdot(K_i\nabla T_i), \tag{14}$$

$$\rho\frac{\mathrm{D}e_e}{\mathrm{D}t} = -p_e\nabla\cdot\boldsymbol{u} + \bar{K_{ie}}(T_i - T_e) + \nabla\cdot(K_e\nabla T_e), \tag{15}$$

with $e = e_i + e_e$, $p = p_i + p_e$, and $\bar{K_{ie}}$, K_i and K_e, the ion-electron coupling, ion and electron thermal conductivities. A is the artificial viscosity.

Alternatively, energy change due to plasma can also be modeled as a source term similar to that in the R-P model in [35],

$$S_e = ... - \sum_i \chi_{red,i}\Delta n_i^+, \tag{16}$$

with $\chi_{red,i}$ being the reduced ionization potential of the gas species i by the extreme high density, and Δn_i^+ the change of the number of positive ions of the species i.

An attempt will be made to include detailed plasma-hydro coupling and plasma chemistry following [33, 34]. In [33, 34], a model was developed for the combustion of hydrogen assisted by plasma generated by dielectric-barrier discharge that includes neutral-neutral, neutral-ion chemistry in local thermodynamics equilibrium and the contribution of electron impact collisions in non-local thermodynamics equilibrium (NLTE) but with the electrons in a quasi-steady state with the background gas and the local electric field. Detailed plasma-hydro coupling and plasma chemistry

are accounted for through source term like that for energy equation,

$$S_T = en_e\mu_e|\nabla\phi|^2 + 2n_e\bar{\epsilon}\frac{m_e}{m_{BG}}\left(1-\frac{T}{T_e}\right)\nu_{M,BG} - \sum_k \dot{\omega}_{cr,k}\Delta E_k. \tag{17}$$

Here, ϕ is the electric potential, μ_e is the electron mobility, $\bar{\epsilon}$ is the mean electron energy, m_{BG} is the mass of the target gas molecules, $\nu_{M,BG}$ is the effective-momentum transfer frequency between electron and target particles, $\dot{\omega}_{cr,k}$ are the inelastic kinetic rates, ΔE_k are the associated inelastic energy loss (per unit mole), and T_e and T are the electron and target gas temperatures, respectively.

5.4 Light Emission Modeling

We first note that coupling of radiation with the hydrodynamics can be done by adding a source term

$$S_e = ... - \nabla\cdot\boldsymbol{q}_r, \tag{18}$$

in the energy equation with $\boldsymbol{q}_r$ being the radiative heat flux. The energy equation then becomes an integro-differential equation since the evaluation of $\nabla\cdot\boldsymbol{q}_r$ comes from an integral equation in temperature [70]. However, typical SBSL spectra like those in [1, 40, 41] can be integrated to show that the energy per flash is on the order of $10^{-9}-10^{-8}$ W while in our simulations in [3] (Fig. 2) the power due to internal energy is on the order of $E_iV_{bub}\sim 1\times10^{-5}$ W. Here, $E_i=\rho e=\Gamma p+\Pi$ with $p\sim10^2$ GPa at the rebound, and the volume of the bubble $V_{bub}\sim100$ μm^3 at the rebound with radius $a\sim3$ μm. Consequently, the photon field cannot affect the matter field. Thus, the coupling of radiation with the hydrodynamics needs not to be considered, and the light emission can be calculated as a post-processing of the flow field from hydrodynamic simulations.

The main processes of sonoluminescence photon emission are (i) bremsstrahlung from inelastic collisions of free electrons with neutral atoms, (ii) bremsstrahlung of free electrons in the field of ions, and (iii) photon emission from the recombination of free electrons and ions to excited atoms [36, 38, 39]. The emitted intensity at wavelength λ for SL with local thermodynamic equilibrium (LTE) approximation follows

$$I_\lambda(s,t) = \int_0^s \kappa_\lambda[T(s',t)]\times exp\left(-\int_0^{s'}\kappa_\lambda[T(s'',t)]ds''\right)I_\lambda^{Pl}[T(s',t)]ds' \tag{19}$$

where $I_\lambda^{Pl}[T(s,t)]$ is the Planck's law emitted intensity approximation for an idealized blackbody and $\kappa_\lambda[T(s,t)]$ is the photon absorption coefficient for a specific wavelength and temperature. Note $\kappa_\lambda[T(s,t)]$ depends on location s and time t through the dependence of temperature. Determining $\kappa_\lambda[T(s,t)]$ is quite involved and the formulas in Hilgenfeldt *et al.* [36] for various contributions are not shown here for brevity. The final absorption coefficient follows [36],

$$\kappa_\lambda[T] = \kappa_\lambda^{ff0}[T] + \kappa_\lambda^{ion}[T] \tag{20}$$

where κ_λ^{ff0} and κ_λ^{ion} are the absorption coefficient due to process (i) and (iii) above, respectively.

Note, just like for water and air chemistry and plasma physics discussed in the previous sections, detailed radiation modeling with transitions between states explicitly modeled as reactions like in [30,71] may also be attempted. In [30], a solution was obtained from a viscous three-dimensional flowfield calculation with reacting water chemistry. The OH flowfield and radiation models were developed. Comparison were then made between calculation and experiments for the spectral data of the shock-heated air surrounding a sounding rocket under flight conditions of 3.5 km/s.

5.5 Comparison with Experiments - Validation and Uncertainty Quantification

Similar to [36–39], spectrum will be computed from the hydrodynamic flow field and the computed spectrum will be compared to the experimental SBSL spectrum such as those in [1,31,40,41] as validation for our integrated framework. For example, the dependence of spectrum of SBSL on acoustic driving pressure shown in Fig. 7 is a good validation test for the overall model with both acoustic excitation and the final collapse stage. In addition, the dependence of observed plasma electron density on acoustic driving pressure again in [1] can be use as a validation test for our plasma modeling.

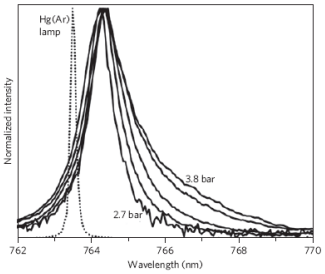

Figure 7: Ar emission line profiles as a function of the acoustic driving pressure, P_a, from [1].

As can be understood, for an integrated framework with a number of models for various physics, uncertainty can have a large impact on modeling accuracy. The uncertainty in numerical simulations may include discretization error, low fidelity model for physics and model parameters, input from experiments, and the propagation of these uncertainties. Therefore, sensitivity analysis will be performed for various uncertain model parameters and "error bar" due to uncertainty will be derived.

5.6 Predictive Modeling for MBSL and Cavitation Erosion

Once the integrated framework is developed and validated with SBSL, the next predictive modeling will be intracavity conditions and bubble interaction in multi-bubble sonoluminesence (MBSL). Also, a broader impact of the proposed research would be cavitation erosion. Acoustic excitation phase in cavitation erosion is typically by-passed due to the larger length and time scale in that phase and the lack of phase transition modeling. Thus, the acoustic excitation simulation for SBSL with the proposed framework provides valuable knowledge base for cavitation erosion. Simulation and research on cavitation process can be done by starting the simulation with acoustic excitation and relaxing the assumption that shock has been generated. Thus, the mechanisms of shock generation and damaging in cavitation erosion may be identified.

6 Broader Impacts

The results from the proposed fundamental research will advance our basic understanding of the nature of fluid dynamics in bubble collapse in sonoluminescence and cavitation erosion. The study of bubble collapse has relevance to a large number of widely varying fields including turbomachinery, naval structures, biomedical ultrasound and shock wave lithotripsy. As a result, the understanding of the mechanisms behind these phenomena will benefit not only the fluid dynamics community but also chemistry, physics, ocean and hypersonic aerospace engineering communities. Note the temperatures in our proposed problem also appear in flows in the hypersonic regime. Therefore, a broader impact of the current proposal is to advance modeling capability in hypersonic flow. In fact, some of the air chemistry data and model in the current work were obtained from aerospace research [30, 68].

The proposed research will support the training of a Postdoctral Fellow and a Ph.D. student as well as a broad educational plan encompassing undergraduate and K-12 students and STEM.

The Postdoctral Fellow and the doctoral student will work closely together on problems at the interface of fluid-thermo science, physics and chemistry, which will foster the next generation of multidisciplinary scientists. To increase exposure and acquire more interest in the topic, class lectures on the research will be offered in Mechanical and Aerospace Engineering. A presentation at Graduate Seminar at FIT is also expected. The student will be exposed to examples of how what they learned in the classroom may be applied to the real-world applications, and numerical methods and leading HPC trends. Lab tours will be offered in summers to K-12 students, and Summer Workshop will be offered to undergraduate students. We have run a week-long Summer Workshop program since 2015. Engineering lectures and lab tours are arranged. The topics covered include general fluid mechanics and thermodynamics, and renewable energy. Results from this research can also be introduced in the Workshop.

The visually appealing results from this work will be disseminated through multimedia outlets to promote STEM, including the Orlando Science Museum. The results from this research will be published in high-impact journals, such as Physical Review - Fluids, Journal of Fluid Mechanics, International journal of multiphase flow etc. and through seminars at interdisciplinary conferences and diverse university departments. This work will be of interest to a broad community, including fluid dynamic, physics, chemistry research community and aerospace industry.

6.1 Methods of Assessment

A variety of methods will be used to assess both the short-term effects and long-term impact of our research and outreach activities. For the possible presentations and demonstrations on SL delivered by the PIs at the Orlando Science Museum, the number of audience members will be recorded and compared to other activities at the Science Museum. When possible, the audience will be asked to evaluate their experience and the impact of the programs on their views of fundamental fluid dynamics, and computational flow visualization via a brief questionnaire. Data from the questionnaires will be compiled and shared with the Science Coordinators at the Science Museum for feedback and refinement of the programs. Similar questionnaires can be used for Summer Workshop as well. In addition, all data pertaining to the participation in the Workshop will be quantified and tabulated. This will include the number and demographics of the participants, the states, and institutions represented, and the manner in which the participants learned of the workshop, among other metrics.

7 Personnel Management

The PI, Dr. Ju Zhang at FIT, will direct the numerical simulation work following the discussion presented in Section 5. Dr. Zhang has extensive experience in numerical simulation of multi-phase and multi-physics applications. Dr. Pei-feng Hsu, co-PI at FIT, will assist radiation and light emission modeling. Dr. Thomas L. Jackson, co-PI at UF in the Department of Mechanical and Aerospace Engineering, will participate in code development and in running the code on appropriate machines at UF. He will participate in preparation of publications of the results from the proposed work. He will also assist the PI in leading the overall effort.

8 Prior NSF Support

Neither the PI nor the co-PIs has received NSF support within the last five years.

References

[1] Flannigan, D. J., and Suslick, K. S. (2010). Inertially confined plasma in an imploding bubble. Nature Physics, 6(8), 598.

[2] Flannigan, D. J., and Suslick, K. S. (2005). Plasma formation and temperature measurement during single-bubble cavitation. Nature, 434(7029), 52.

[3] Zhang, J., Jackson, T. L., and Jost, A. M. D. (2017). Effects of air chemistry and stiffened EOS of air in numerical simulations of bubble collapse in water. Physical Review Fluids, 2(5), 053603.

[4] Marinesco, N. and Trillat, J.J. (1933). Action of supersonic waves upon the photographic plate. Proc R Acad Sci, Vol. 196, pp. 858-860.

[5] Frenzel, J. and Schultes, H. (1934). Luminescence in water carrying supersonic waves. Z. Phys. C, Vol. 27, pp. 421-424.

[6] Rayleigh, L. (1917). VIII. On the pressure developed in a liquid during the collapse of a spherical cavity. The London, Edinburgh and Dublin Philosophical Magazine and Journal of Science, Vol. 34(200), pp. 94-98.

[7] Plesset, M.S. (1949). The dynamics of cavitation bubbles. Journal of applied mechanics, Vol. 16, pp. 277-282.

[8] Hilgenfeldt, S., Brenner, M.P., Grossmann, S. and Lohse, D. (1998). Analysis of Rayleigh-Plesset dynamics for sonoluminescing bubbles. Journal of fluid mechanics, Vol. 365, pp. 171-204.

[9] Putterman, S., Evans, P.G., Vazquez, G. and Weninger, K. (2001). Cavitation science: Is there a simple theory of sonoluminescence?. Nature, Vol. 409(6822), pp. 782-783.

[10] Brenner, M.P., Hilgenfeldt, S. and Lohse, D. (2002). Single-bubble sonoluminescence. Reviews of modern physics, Vol. 74(2), pp. 425.

[11] Suslick, K.S. and Flannigan, D.J. (2008). Inside a collapsing bubble: sonoluminescence and the conditions during cavitation. Annu. Rev. Phys. Chem., Vol. 59, pp. 659-683.

[12] Vignoli, L.L., De Barros, A.L., Thom, R.C., Nogueira, A.L.M.A., Paschoal, R.C. and Rodrigues, H. (2013). Modeling the dynamics of single-bubble sonoluminescence. European Journal of Physics, Vol. 34(3), pp. 679.

[13] Lauterborn, W. and Kurz, T. (2010). Physics of bubble oscillations. Reports on progress in physics, Vol. 73(10), 106501.

[14] Yasui, K. (1997). Alternative model of single-bubble sonoluminescence. Physical Review E, 56(6), 6750.

[15] Yasui, K., Tuziuti, T., Sivakumar, M., and Iida, Y. (2005). Theoretical study of single-bubble sonochemistry. The Journal of chemical physics, 122(22), 224706.

[16] Yasui, K., Tuziuti, T., Lee, J., Kozuka, T., Towata, A. and Iida, Y. (2010). Numerical simulations of acoustic cavitation noise with the temporal fluctuation in the number of bubbles. Ultrasonics sonochemistry, Vol. 17(2), pp. 460-472.

[17] Schanz, D., Metten, B., Kurz, T., and Lauterborn, W. (2012). Molecular dynamics simulations of cavitation bubble collapse and sonoluminescence. New Journal of Physics. 14, 113019.

[18] Tsiglifis, K. and Pelekasis, N.A. (2007). Numerical simulations of the aspherical collapse of laser and acoustically generated bubbles. Ultrasonics sonochemistry, Vol. 14(4), pp. 456-469.

[19] Alhelfi, A. and Sundn, B. (2015). A condition monitoring for collapsing bubble mechanism for sonoluminescence and sonochemistry. Journal of Thermal Science and Engineering Applications, Vol. 7(2), 021014.

[20] Prosperetti, A. (2017). Vapor Bubbles. Annual Review of Fluid Mechanics, 49, 221-248.

[21] Wu, C.C. and Roberts, P.H. (1993). Shock-wave propagation in a sonoluminescing gas bubble. Physical review letters, Vol. 70(22), pp. 3424.

[22] Moss, W.C., Clarke, D.B., White, J.W. and Young, D.A. (1994). Hydrodynamic simulations of bubble collapse and picosecond sonoluminescence. Physics of Fluids, Vol. 6(9), pp. 2979-2985.

[23] Moss, W. C., Clarke, D. B., and Young, D. A. (1997). Calculated pulse widths and spectra of a single sonoluminescing bubble. Science, 276(5317), 1398-1401.

[24] Zhang, J., Jackson, T.L., Buckmaster, J.D. and Freund, J.B. (2012). Numerical modeling of shock-to-detonation transition in energetic materials. Combustion and Flame, Vol. 159(4), pp. 1769-1778.

[25] Sridharan, P., Jackson, T.L., Zhang, J. and Balachandar, S. (2015). Shock interaction with one-dimensional array of particles in air. Journal of Applied Physics, Vol. 117, 075902.

[26] Shukla, R.K., Pantano, C. and Freund, J.B. (2010). An interface capturing method for the simulation of multi-phase compressible flows. Journal of Computational Physics, Vol. 229(19), pp. 7411-7439.

[27] Saurel, R., Petitpas, F., and Abgrall, R. (2008). Modelling phase transition in metastable liquids: application to cavitating and flashing flows. Journal of Fluid Mechanics, 607, 313-350.

[28] Saurel, R., Petitpas, F., and Berry, R. A. (2009). Simple and efficient relaxation methods for interfaces separating compressible fluids, cavitating flows and shocks in multiphase mixtures. Journal of Computational Physics, 228(5), 1678-1712.

[29] Zein, A., Hantke, M., and Warnecke, G. (2010). Modeling phase transition for compressible two-phase flows applied to metastable liquids. Journal of Computational Physics, 229(8), 2964-2998.

[30] Levin, D. A., Collins, R. J., Candler, G. V., Wright, M. J., and Erdman, P. W. (1996). Examination of OH ultraviolet radiation from shock-heated air. Journal of thermophysics and heat transfer, 10(2), 200-208.

[31] Flannigan, D. J., and Suslick, K. S. (2005). Plasma line emission during single-bubble cavitation. Physical review letters, 95(4), 044301.

[32] Zeldovich, Y.B. and Raizer, Y.P., Physics of Shock Waves and High-Temperature Hydronamic Phenomena (Academic Press, New York, 1966).

[33] Massa, L. L., and Freund, J. B. (2016). An integrated predictive simulation model for the plasma-assisted ignition of a fuel jet in a turbulent crossflow. In 54th AIAA Aerospace Sciences Meeting (p. 2154).

[34] Massa, L., and Freund, J. B. (2017). A Model for Plasma-Combustion Coupling and its Effect on the Ignition of a Dielectric-Barrier Discharge Actuated Hydrogen Jet. In 55th AIAA Aerospace Sciences Meeting (p. 0391).

[35] Yasui, K. (2001). Effect of liquid temperature on sonoluminescence. Physical Review E, 64(1), 016310.

[36] Hilgenfeldt, S., Grossmann, S., and Lohse, D. (1999). Sonoluminescence light emission. Physics of Fluids, 11(6), 1318-1330.

[37] Yasui, K. (1999). Mechanism of single-bubble sonoluminescence. Physical Review E, 60(2), 1754.

[38] Jeon, J. S., Yang, I. J., Na, J. H., and Kwak, H. Y. (2000). Radiation mechanism for a single bubble sonoluminescence. Journal of the Physical Society of Japan, 69(1), 112-119.

[39] Byun, K. T., Kwak, H. Y., and Karng, S. W. (2004). Bubble evolution and radiation mechanism for laser-induced collapsing bubble in water. Japanese journal of applied physics, 43(9R), 6364.

[40] Hiller, R., Putterman, S. J., and Barber, B. P. (1992). Spectrum of synchronous picosecond sonoluminescence. Physical Review Letters, 69(8), 1182.

[41] Hiller, R., Weninger, K., Putterman, S. J., and Barber, B. P. (1994). Effect of noble gas doping in single-bubble sonoluminescence. Science, 266(5183), 248-250.

[42] Hawker, N.A. and Ventikos, Y. (2012). Interaction of a strong shockwave with a gas bubble in a liquid medium: a numerical study. Journal of Fluid Mechanics, Vol. 701, pp. 59-97.

[43] Niederhaus, J.H., Greenough, J.A., Oakley, J.G., Ranjan, D., Anderson, M.H. and Bonazza, R. (2008). A computational parameter study for the three-dimensional shockbubble interaction. Journal of Fluid Mechanics, Vol. 594, pp. 85-124.

[44] Ranjan, D., Niederhaus, J.H., Oakley, J.G., Anderson, M.H., Bonazza, R. and Greenough, J.A. (2008). Shock-bubble interactions: Features of divergent shock-refraction geometry observed in experiments and simulations. Physics of Fluids (1994-present), Vol. 20(3), 036101.

[45] Bourne, N.K. and Milne, A.M. (2003, August). The temperature of a shock-collapsed cavity. In Proceedings of the Royal Society of London A: Mathematical, Physical and Engineering Sciences (Vol. 459, No. 2036, pp. 1851-1861). The Royal Society.

[46] Tully, B., Hawker, N. and Ventikos, Y. (2016). Modeling asymmetric cavity collapse with plasma equations of state. Physical Review E, Vol. 93(5), 053105.

[47] Johnsen, E. and Colonius, T. (2008). Shock-induced collapse of a gas bubble in shockwave lithotripsy. The Journal of the Acoustical Society of America, Vol. 124(4), pp. 2011-2020.

[48] Johnsen, E. and Colonius, T. (2009). Numerical simulations of non-spherical bubble collapse. Journal of fluid mechanics, Vol. 629, pp. 231-262.

[49] Toro, E.F. (2013). Riemann solvers and numerical methods for fluid dynamics: a practical introduction. Springer, Berlin.

[50] Toro, E.F., Spruce, M. and Speares, W. (1994). Restoration of the contact surface in the HLL-Riemann solver. Shock waves, Vol. 4(1), pp. 25-34.

[51] Gottlieb, S. and Shu, C.W. (1998). Total variation diminishing Runge-Kutta schemes. Mathematics of computation of the American Mathematical Society, Vol. 67(221), pp. 73-85.

[52] Tiwari, A., Freund, J.B. and Pantano, C. (2013). A diffuse interface model with immiscibility preservation. Journal of computational physics, Vol. 252, pp. 290-309.

[53] Shukla, R.K. (2014). Nonlinear preconditioning for efficient and accurate interface capturing in simulation of multicomponent compressible flows. Journal of Computational Physics, Vol. 276, pp. 508-540.

[54] Zhang, J., Jackson, T. L., Sridharan, P., and Balachandar, S. (2017, January). Towards a mass and volume conserving interface reinitialization scheme for a diffuse interface methodology (for shock-particle interaction). In AIP Conference Proceedings (Vol. 1793, No. 1, p. 150005). AIP Publishing.

[55] Allaire, G., Clerc, S. and Kokh, S. (2002). A five-equation model for the simulation of interfaces between compressible fluids. Journal of Computational Physics, Vol. 181(2), pp. 577-616.

[56] Schott, G.L (1983). Measured Hugoniot States of a Two-elements Fluid, O_2 + N_2, near 2 Mg/m^3, in Shock Waves in Condensed Matter (1983), J.R. Asay, R.A. Graham, G.K. Struab (editors).

[57] Lubachevsky, B.D. and Stillinger, F.H. (1990). Geometric properties of random disk packings. Journal of statistical Physics, Vol. 60(5-6), pp. 561-583.

[58] Maggi, F., Stafford, S., Jackson, T.L. and Buckmaster, J. (2008). Nature of packs used in propellant modeling. Physical Review E, Vol. 77(4), 046107.

[59] Jackson, T.L., Hooks, D.E. and Buckmaster, J. (2011). Modeling the microstructure of energetic materials with realistic constituent morphology. Propellants, Explosives, Pyrotechnics, Vol. 36(3), pp. 252-258.

[60] Keller, J.B. and Miksis, M.(1980). Bubble oscillations of large amplitude. J. Acoust. Soc. Am., 68(2), 628-633.

[61] Sun, M., Saito, T., Takayama, K. and Tanno, H. (2004). Unsteady drag on a sphere by shock wave loading. Shock Waves, Vol. 14, pp. 3-9.

[62] Suslick, K.S., Doktycz, S.J. and Flint, E.B. (1990). On the origin of sonoluminescence and sonochemistry. Ultrasonics, 28(5), pp. 280-290.

[63] Bell, J., Almgren, A., Beckner, V., Day, M., Lijewski, M., Nonaka, A. and Zhang, W. (2012). BoxLib users guide.

[64] Jost, A.M.D., Zhang, J. and Jackson, T.L. Incompressible Flow Solver with Ghost-Cell Immersed Boundary Method and Adaptive Mesh Refinement. AIAA-paper-2016-3328.

[65] Kapila, A. K., Menikoff, R., Bdzil, J. B., Son, S. F., and Stewart, D. S. (2001). Two-phase modeling of deflagration-to-detonation transition in granular materials: Reduced equations. Physics of fluids, 13(10), 3002-3024.

[66] Baer, M. R., and Nunziato, J. W. (1986). A two-phase mixture theory for the deflagration-to-detonation transition (DDT) in reactive granular materials. International journal of multiphase flow, 12(6), 861-889.

[67] Simoes-Moreira, J. R., and Shepherd, J. E. (1999). Evaporation waves in superheated dodecane. Journal of Fluid Mechanics, 382, 63-86.

[68] Anderson, J.D. (2000). Hypersonic and high temperature gas dynamics. AIAA.

[69] Borgnakke, C. and Sonntag, R.E. Fundamentals of Thermodynamics, 8th edition. John Wiley & Sons, 2013.

[70] Modest, M. F. (2013). Radiative heat transfer. Academic press.

[71] Zhang, J., Goldstein, D. B., Varghese, P. L., Gimelshein, N. E., Gimelshein, S. F., and Levin, D. A. (2003). Simulation of gas dynamics and radiation in volcanic plumes on Io. Icarus, 163(1), 182-197.